Hindawi
Advances in Materials Science and Engineering
Volume 2023, Article ID 9852428, 1 page
https://doi.org/10.1155/2023/9852428

Retraction

Retracted: Image-Based Precision Measurement Technology for the Quality Inspection of Crane Boom Materials

Advances in Materials Science and Engineering

Received 26 December 2023; Accepted 26 December 2023; Published 29 December 2023

This article has been retracted by Hindawi, as publisher, following an investigation undertaken by the publisher [1]. This investigation has uncovered evidence of systematic manipulation of the publication and peer-review process. We cannot, therefore, vouch for the reliability or integrity of this article.

Please note that this notice is intended solely to alert readers that the peer-review process of this article has been compromised.

Wiley and Hindawi regret that the usual quality checks did not identify these issues before publication and have since put additional measures in place to safeguard research integrity.

We wish to credit our Research Integrity and Research Publishing teams and anonymous and named external researchers and research integrity experts for contributing to this investigation.

The corresponding author, as the representative of all authors, has been given the opportunity to register their agreement or disagreement to this retraction. We have kept a record of any response received.

References

[1] H. Liu, W. Tan, S. Cao, and H. Li, "Image-Based Precision Measurement Technology for the Quality Inspection of Crane Boom Materials," *Advances in Materials Science and Engineering*, vol. 2022, Article ID 8379621, 13 pages, 2022.

Hindawi
Advances in Materials Science and Engineering
Volume 2022, Article ID 8379621, 13 pages
https://doi.org/10.1155/2022/8379621

Research Article

Image-Based Precision Measurement Technology for the Quality Inspection of Crane Boom Materials

Honghua Liu, Wenping Tan, Shen Cao, and Hongmei Li

College of Information and Mechatronical Engineering, Hunan International Economics University, Changsha 410205, Hunan, China

Correspondence should be addressed to Wenping Tan; tanwenp2004@163.com

Received 7 July 2022; Revised 16 August 2022; Accepted 6 September 2022; Published 27 September 2022

Academic Editor: K. Raja

With the slow rise of the construction industry, cranes, as indispensable mechanical equipment in construction projects, are widely used in the lifting and handling of specific space ranges of construction projects. The quality of crane booms is particularly important for safety. This paper uses image measurement methods including filter processing, mean filtering, and Gaussian filtering to detect the quality of the crane boom material. The image is processed by the wavelet transform and Fourier transform. The grayscale transformation stretching method is applied to the surface image analysis of the boom material to obtain the final inspection. The research results show that the use of image measurement methods can effectively measure the thickness of the crane boom material, the geometric information of the boom material, and the surface roughness of the material and obtain effective image information. The detection accuracy reaches 98.1%. The error can be controlled better. The inspection and research on the quality of crane jib materials can ensure the quality and performance of crane jib materials, reduce the potential safety hazards of cranes during operation, and improve safety. This article organically combines workpiece surface roughness detection with digital image processing technology to preprocess the surface picture of the arm tube material. On this basis, the texture features in the image are extracted and programmed to calculate, and the final workpiece is obtained by the surface roughness value, which proves the feasibility of this method. The research results have very important practical significance for the detection of the quality of the arm tube material and the improvement of the quality level of the arm tube material.

1. Introduction

With the development of large-scale production of machinery industrialization, people's requirements and industrial demands have put forward higher standards for the accuracy of products and the quality of materials. Because the detection accuracy, detection speed, quality, and other aspects of contact measuring instruments need to be improved, the noncontact nondestructive testing technology is promoted. Among the detection methods, digital image processing technology belongs to noncontact detection technology, so it is also nondestructive detection technology. It has important prospects in the development of machinery industry. In the machinery industry, surface roughness is used to evaluate the microscopic geometric characteristics of the workpiece surface after processing. It is a very important index in mechanical processing and it is also used to characterize the surface quality of the workpiece. In the field of industrial production, especially in various manufacturing industries, such as ultraprecision machinery, instrumentation and rolling bearings, the theory, technology, and methods of surface roughness detection of workpieces have also received extensive attention in the research field. The key technologies such as collecting, processing, filtering, and random measurement of free-form surface measurement of the original data of parts and components have been studied systematically and in depth. In the early days of cloud computing, it was simply distributed computing that solved

task distribution and performed merging of computational results. Thus, cloud computing is also known as grid computing.

The surface roughness of mechanical parts is also called the surface finish of the workpiece. It is used to evaluate the machined surface and is a common parameter for various tiny machining traces. In the process of forming parts, the size and shape of the parts belong to the macrosize, while the small unevenness of the image surface belongs to the microgeometric characteristics. This processing trace is called the microgeometric shape error. In the field of mechanical development, surface roughness measurement is a precise and high-precision detection technology, which is the basis and prerequisite for the development of the machinery industry at this stage. From the perspective of the machining and development direction of the machinery industry, the improvement of machining accuracy is closely related to surface quality inspection technology. The inspection accuracy and efficiency of surface quality can affect the level of processing technology in a large way. To ensure the clarity of image magnification, a microscope was used here for image observation.

High-precision mass measurement is very important for precise motion control of cranes. Li et al. [1] considered the uncertain factors in the optimization design of crawler crane truss boom and solved the reliability-based design optimization (RBDO) problem involving discrete design variables and multiple working condition constraints. In the optimization model, the uncertainty of material properties, geometric parameters, and loads are represented by random variables. The geometric dimensions, the reliability index of the performance function, and the minimum weight of the truss arm are, respectively, defined as random design variables, probability constraints, and objective functions. Combining the reliability analysis method based on the response surface method (RSM) with the multi-island genetic algorithm (MIGA), an efficient reliability-based lattice boom design optimization process was developed under typical constrained conditions. Several verification cases are given to prove the effectiveness of the optimization results. The results show that the reliability-based design optimization method can not only meet the reliability constraints of the lattice arm but also ensure the reliability of the structure [1]. Trevino et al. [2] provide additional important considerations for tower crane allocation issues. The main contribution of their work to the knowledge system is to model the relationship between the tower crane's load capacity and its associated costs. However, in these models, the authors unfortunately incorporated some shortcomings into their new model without any modification [2]. Yao et al. [3] established the differential equation of n-th order section telescopic boom based on the continuous beam-column theory. The recursive formula for the stability of the n-th order telescopic boom is derived by mathematical induction. The numerical optimization algorithm combined with mechanical characteristics is used to solve the transcendental equation in the recursive formula and to determine the equation when n is unknown. The obtained length coefficient is compared with the length coefficient calculated by Chinese national standard GB3811-2008 and ANSYS 17.0. The results show that the accuracy of the Levenberg–Marquardt algorithm is better than other algorithms. Moreover, the obtained length coefficient shows a certain degree of nonlinearity. Therefore, linear interpolation is feasible in small-scale practical applications. The use of linear interpolation leads to a large error in the n-stage critical force of the all-terrain crane [3]. Sun et al. [4] proposed a high-precision calibration method. Instead of using a large 3D pattern, he uses a small flat pattern and a precalibrated matrix camera to obtain a large number of appropriately distributed points, which will ensure the accuracy of the calibration results. The matrix camera eliminates the need for precise adjustment and movement and can easily connect the line scan camera with the world, both of which enhance the flexibility of the measurement field. This method has been verified by experiments. Experimental results show that the proposed method provides a practical solution for calibrating the line scan camera for accurate measurement [4]. In the image measurement method, Zemann et al.'s [5] spectral shape of 32P has been carefully remeasured in the magnetic intermediate image spectrometer. The source is produced in a mass separator to improve source quality and remove 33P. The interference effects that may be caused by non-ideal magnetic fields and various baffles, sources, and source supports are measured, and upper limits are set for various effects. An improved light source holder with little scattering and an improved scintillation detector with a background elimination function are used. Small corrections were made to the limited resolution and backscatter from the scintillator and source foil. Contrary to many published results, he obtained the shape factor coefficients, that is, the statistical spectrum shape and the error comes from the estimation of possible but undetected interference effects [5]. Yuan and Huang [6] proposed an angle measurement algorithm. By analyzing the characteristics of the edge of the raster image, a fast method of using three gradient points to establish a parabolic function is applied to the automatic detection of the subpixel edge of the raster image, and the coarse code decoding is improved to reduce the bit error rate (BER) and manufacturing difficulty. A high-precision subdivision method based on the grating line observation image is introduced to calculate the subdivision angle. Second, BER simulation and accuracy analysis show that the algorithm has robustness, reliability, and accuracy in both the coarse code decoding and subdivision processes [6]. Jing et al. [7] proposed a high-precision and stable mover position detection method based on time image correlation and fence image. First, the linear motor positioning system is used to record the sequence of fence images with mover position information, and the integer pixel displacement of each image is obtained through the image correlation method. Then, according to the continuity of the motion, the subpixel displacement can be extracted by fitting the integer pixel displacement. Finally, the displacement and velocity curves can be calculated according to the system calibration. Compared with the digital image

measurement used for linear motor position detection, this method can accurately detect the position of the mover, the measurement range is longer, and the uncertainty is smaller. The moving least squares (MLS) algorithm is used to ensure the stability of measurement uncertainty in different motion modes [7].

The innovation of this paper is that the image-based measurement technology uses the wavelet transform profilometry of the Morlet wavelet to obtain the phase value of the moiré image. By analyzing the advantages and disadvantages of the point-by-point unwrapping algorithm, the branch-and-cut method, and the quality map-guided method, the branch-and-cut method is finally decided as the unwrapping algorithm for the truncated phase. Finally, it is improved on the basis of the Gaussian low-pass filter, and the reconstructed material surface is analyzed, which can effectively reduce the surface error of the arm tube material caused by the reconstruction algorithm and improve the accuracy of detection. It can be seen that the method of digital analysis of material surface map in this paper has higher accuracy, faster computing speed, and lower requirement for experimental equipment compared with the traditional method.

2. Detection Method of Crane Boom Material Quality Based on Image-Based Precision Measurement

2.1. Image Preprocessing. In the process of computer processing images, the process of image denoising, filtering, segmentation, etc., is called image preprocessing [8, 9]. The principle of intelligent image processing is shown in Figure 1. It can clear the picture, remove the interference information in the picture, make the computer get the purpose information more clearly, and enhance the required information in the picture, and then segment the image, as well as various processing such as image enhancement and image extraction [10, 11].

First, we determine whether there is a first distribution label-matching initial saliency evaluation in the previously acquired scene image; if so, we determine an auxiliary saliency evaluation for determining whether a target face is an abnormal target face by the first distribution label-matching initial saliency evaluation previously acquired and said saliency evaluation, determining whether said target face is an abnormal target face by said auxiliary saliency evaluation, and tagging the auxiliary saliency evaluation to said scene image as a first distribution label-matching initial saliency evaluation when the target face is not an abnormal target face.

In the actual operation process, image preprocessing is essential, but before preprocessing, the image is generally grayed out first, and then, the analysis calculation is started. For color images, grayscale images contain less information, are clearer, and are more convenient to process and extract the required information. In the process of computer processing, there are generally four methods to convert it into grayscale images [12].

2.1.1. Component Method. In the internal practice of image processing, it is necessary to select the gray value from the three colors of the color image, use the brightness of the three components as three gray levels, and then select the gray level according to the needs of the calculation itself to generate gray degree image.

$$\begin{aligned} K_1(s,t) &= R(s,t), \\ K_2(s,t) &= G(s,t), \\ K_3(s,t) &= B(s,t). \end{aligned} \tag{1}$$

The function $K_x(s,t)(x = 1, 2, 3)$ can be regarded as the gray value of each pixel after grayscale processing.

2.1.2. Maximum Method. The maximum value method is in the internal practice of image processing, and the gray value is selected as the gray value of the three colors with the highest brightness.

$$K(s,t) = \max\left(R(s,t), G(s,t), B(s,t)\right). \tag{2}$$

2.1.3. Average Method. When the image is grayed out, the gray value is the average of the three brightness values in the original image. This method can be called the average value method.

$$K(s,t) = \left(R(s,t), G(s,t), B(s,t)\right)/3. \tag{3}$$

2.1.4. Weighted Average Method. In real life, the most sensitive eye color of the human eye is green and the least sensitive is blue. The three components are added with different weights and the weights are averaged.

$$K(s,t) = 0.5 * R(s,t), 0.58 * G(s,t), 0.16 * B(s,t). \tag{4}$$

2.2. Image Noise Reduction. In the process of image processing, due to many reasons, the image contains noise. Whether it is internal or external noise, it needs to be filtered to reduce noise to improve image quality [13, 14], and in the actual noise reduction process. In this case, it may cause the image to be blurred, so the image target information is more unclear and the image quality is reduced. Of course, for some filtering methods, the phenomenon of image blur will not appear, so different filtering processing should be carried out for different images [15, 16].

The image sampling process often determines the image quality. The image sampling process will affect the image quality not only because of the external environment such as temperature and dust but also because of the transmission mode, the compression mode, and transmission medium of the image during transmission, so as to hinder the machine or people from obtaining the target information [17, 18]. Due to the interference of noise, images often have problems such as image blur, image degradation, and unclear image features, which cause great trouble to analyze images, and low-quality images are difficult to meet people's

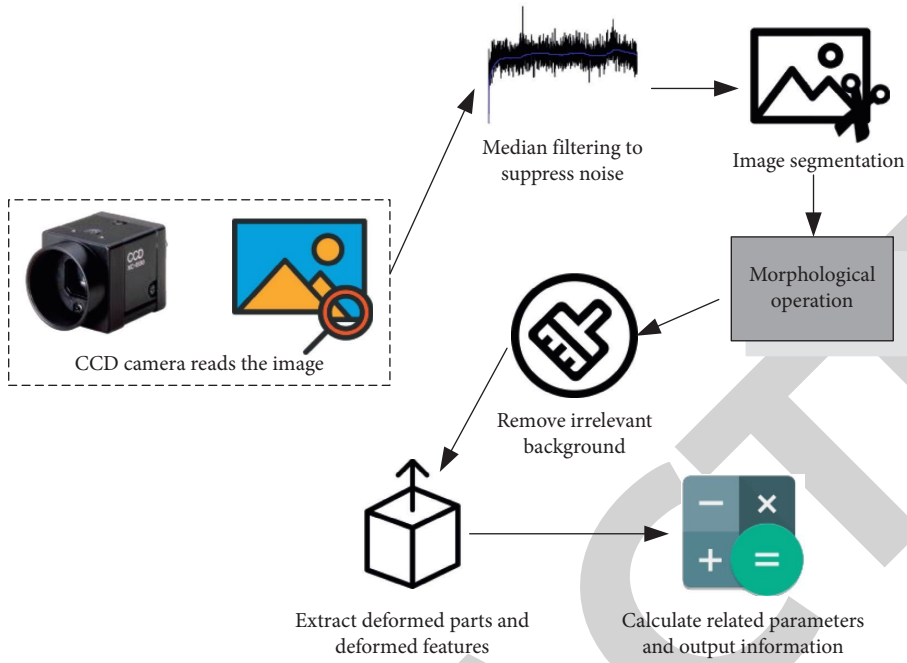

Figure 1: Principle of the intelligent image processing method.

requirements [19, 20]. In the target identification and tracking of images, such images are also very difficult [21]. In real life, it is very important to suppress all kinds of noise signals that degrade the image, enhance the favorable information in the image, and process and correct the detected different images under the same constraint [22, 23].

2.2.1. Filter Processing. In the analysis and calculation, there is a distinction between the spatial domain and the frequency domain. To enhance the quality of the image in the spatial domain, it is necessary to perform image processing on the image [24, 25]. The essence of image processing is to calculate and analyze each pixel in the image. In the calculation and analysis of pixels, the calculation and analysis of a single pixel is a point operation and the calculation and analysis of the pixels in the entire template is a block operation [26, 27]. In actual operation, point operations can be performed, pixels can be separated and unrelated, and block operations can be performed. When each block is calculated and analyzed, it is unrelated to other pixels [28]. By operating on the pixels, you can change the contrast and grayscale distribution of the picture. If you are processing images, if you need to perform grayscale transformation, histogram correction, and grayscale adjustment, you can choose point operation. If you need to smooth and sharpen the picture, you can perform block operations and it can also smooth the outline of the image. There are many methods for image smoothing; the most commonly used is the median and mean filtering methods, and of course, there are many other methods [29, 30].

The median filter can be expressed by formula (5):

$$D(i,j) = median\{f(i-a, j-b)\}(i,j) \in w, \quad (5)$$

where $D(i,j)$ is the pixel gray value of the image output, $f(i-a, j-b)$ is the pixel gray value of the image input, and the template window w. In the process of calculation and analysis, the median filter also needs a template to calculate and analyze the image. The shape of the template can also be various, such as a circle, a cross, and a square.

2.2.2. Mean Filtering. Mean filtering is also called neighborhood averaging, which is replaced by the average value of all pixels in a template placed on a single pixel. In the actual operation of image processing, mean filtering is often used in image processing. It can not only reduce noise but also improve image quality. Mean filtering is also divided into many kinds of filters for selection. In actual operation, when selecting various mean filters, they should also be selected according to the conditions of the image itself, so as to better achieve the desired effect.

2.2.3. Gaussian Filtering. Gaussian filtering can eliminate the Gaussian noise and can often be used in the process of noise reduction. The formula is as follows:

$$S(i,j) = \frac{1}{2\pi\partial^2} e^{(i^2+j^2)/2\partial^2}. \quad (6)$$

In actual application, the formula can be transformed as follows:

$$S(a,b) = \frac{1}{2\pi\partial^2} e^{-((i-a-1)+(j-a-1)/2\partial^2)}. \quad (7)$$

The parameter ∂ determines the smoothness of the Gaussian filter, so the parameter ∂ is related to the

smoothness of the image. In practical applications, the larger the parameter ∂, the smoother the image.

2.2.4. Sharpening Filter. In digital image processing, all processing techniques are completed around increasing image quality and meeting visual requirements. Therefore, most image processing will remove noise and then improve the image quality, so that the target image is displayed clearly. Here is a filtering method, namely, the Laplacian operator. If an image is $D(i, j)$, then the Laplacian change is as follows:

$$\nabla^2 D = \frac{\gamma^2 D}{\gamma i^2} + \frac{\gamma^2 D}{\gamma i^2}. \tag{8}$$

Formula (8) can be defined as follows:

$$\frac{\gamma^2 D}{\gamma i^2} = d(i+1, j) + D(i-1, j) - 2D(i, y), \tag{9}$$

$$\frac{\gamma^2 D}{\gamma j^2} = d(i, j+1) + D(i, j+1) - 2D(i, y). \tag{10}$$

It can be seen from formula (10) that Laplace transform also belongs to a kind of linear transform. The Laplace transform is also divided into different transformation methods, which can be divided into discrete and nondiscrete methods. Different processing methods will make the noise of the images different, and there may be no way to use the software to analyze the images with different noise, and the results of the arm tube quality inspection will be affected. The transformation formula for discrete methods is shown in formula (11):

$$\nabla^2 D = D(i+1, j) + D(i-1, j) + D(i, j+1) + D(i, j-1) - 4D(i, j). \tag{11}$$

Image detection is also sometimes used to retrieve a given sub-image from a known image. In the actual calculation and analysis of digital image technology, the principle of the Laplace transform can be used to calculate and analyze the image, which not only improves the digital image technology but also uses this technology to reduce the noise of the image and improve the quality of the image. After the image is processed by the principle of the Laplace transform, the sharpening effect of the image can be retained and the effect of the image can be more obvious. In the processed image, the background and target of the image can be more contrasted. Therefore, the Laplace transform principle is often used in the preprocessing of the image.

The formula of the Laplace transform is as follows:

$$T(i, j) = D(i, j) - \nabla^2 D(x, y), \tag{12}$$

$$T(i, j) = D(i, j) + \nabla^2 D(x, y). \tag{13}$$

If the central coefficient of the Laplace operator is positive, we use (13) to calculate, and if the central coefficient is negative, we use (12) to calculate.

2.3. Fourier Profilometry. The formula of the Fourier profilometry is as follows:

$$A(i, j) = x(i, j) + y(i, j)^e + y^*(i, j)^e, \tag{14}$$

where $x(i, j)$ is the background light intensity of the picture, $y(i, j)$ is the image contrast, and the formula is Fourier transformed with x as a variable,

$$F[A(i, j)] = x(f, j) + y(f - f_0, j) + y^*(f - f_0, j). \tag{15}$$

Among them, $F[A(i, j)]$, $x(f, j)^e$, $y(f - f_0, j)$, and $y^*(f - f_0, j)^e$ are the Fourier spectra of $A(i, j)$, $x(i, j)^e$, $y(i, j)$, and $y^*(i, j)$, respectively.

$$y(f - f_0, j) + y^*(f - f_0, j) = G(f, j) * F(A(i, j)). \tag{16}$$

Among them, $G(f, j)$ is the band pass filter.

We use it as an inverse Fourier transforms to get $2y(i, j)$ and find the phase.

$$\mu(i, j) = \arctan\left[\frac{lm(y(i, j))}{\mathrm{Re}(y(i, j))}\right]. \tag{17}$$

Through the above comparative analysis, it is known that phase-shift profiling uses at least three moiré images to solve the phase (there is a fixed phase difference between the two moiré images). Four moiré images resolve the phase of the moiré, so the processing time of the image is relatively long and cannot meet the online detection of the arm tube material. Although the processing accuracy of the Fourier profiling is not as good as phase-shifting profiling, it only needs one moiré image to extract the phase information of the moiré image, so it has a great advantage in processing speed. Therefore, the Fourier profilometry can better meet the speed requirements of online detection systems. The carbon fiber boom achieves a lightweight design for the pump truck boom, allowing the long reach boom to be put into larger scale use.

2.4. Wavelet Transform Profilometry. Since the Fourier transform was discovered and used, it has solved many signal processing problems, but it has certain limitations. The wavelet transforms studies the limitations of the Fourier transform. It can provide a window those changes with frequency to analyze the characteristics of certain problems globally or locally. It is an ideal tool for signal processing or image processing. Therefore, wavelet transform has attracted people's attention, and its application range is getting wider and wider. Highly accurate images and phase-shift estimates can be obtained using phase correlation calculation methods to reduce phase errors at low resolutions.

There are many common wavelet basis functions, such as Haar wavelet, Mexican hat wavelet, and Morlet wavelet. They have different characteristics. Therefore, it is particularly important to choose an appropriate wavelet basis function. The letter a represents the frequency.

2.4.1. Haar Wavelet. The mathematician Haar proposed the Haar orthogonal set in 1910, which is defined as follows:

$$\psi_s(a) = \begin{cases} 1\, 0 \le a \le \frac{1}{2}, \\ -1\, \frac{1}{2} \le a \le 1, \\ 0\, other. \end{cases} \tag{18}$$

In actual calculations, such as shifting t, the Haar wavelet is orthogonal, and it can be regarded as a difference operation and in the final result, the wavelet function can give the difference between the parts that is not equal to the observed average value. Since the Haar wavelet has no continuity in the time domain, it will be limited when analyzing actual signals and its performance as a basic wavelet is not good. The grayscale histogram is a function of gray levels, which indicates the number of pixels in an image with a certain gray level.

2.4.2. Mexican Hat Wavelet. The Chinese name of Mexican hat wavelet is "Mexico's straw hat" wavelet, which can also be called the Marr wavelet. The Mexican hat function is the second derivative of the Gauss function, which is defined as follows:

$$\psi(a) = \left(1 - a^2\right) e^{-\left(a^2/2\right)}. \tag{19}$$

Because it is shaped like a Mexican sombrero in time domain, it is named after it. The Mexican straw hat wavelet function belongs to the second derivative of the Gaussian function, and it has a good localization function in the time domain and frequency domain.

2.4.3. Morlet Wavelet.

$$\psi(a) = \frac{1}{\sqrt{\pi t_b}} \exp\left(x 2\pi t_b i - \frac{a^2}{t_b} \right), \tag{20}$$

where t_c represents the center frequency of the wavelet, and t_b represents the bandwidth parameter. We select specific parameter values according to actual conditions.

The Morlet wavelet is a sine function under Gaussian envelope. As shown in Figure 2, compared with other wavelet bases, the Morlet wavelet is more similar to the projected sine image. At the same time, the Morlet wavelet has relatively better frequency domain analysis ability and phase extraction effect.

3. Image-Based Precision Measurement of the Crane Boom Material Quality Inspection Experiment

3.1. Crane Boom Material Quality Inspection Experiment. The experimental steps are to obtain the 3D profile of the crane boom material, then collect the grayscale value of the moiré image, and finally perform the grayscale stretch

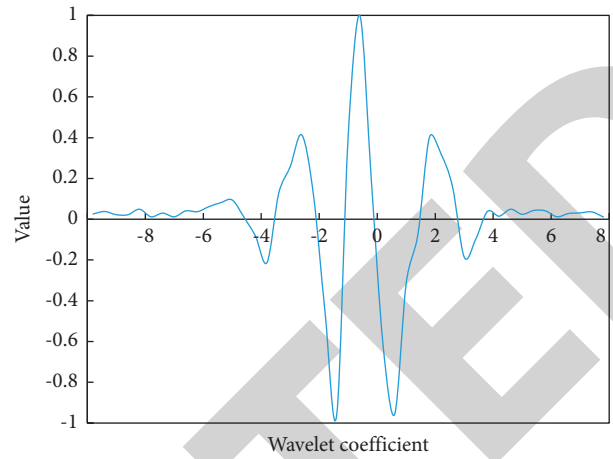

Figure 2: Morlet wavelet time-domain waveform.

transformation. The research in this paper is to detect the quality of crane boom materials. The results of this part of the experiment apply to the filtering algorithm mentioned in the previous section. Common crane boom materials are shown in Table 1.

The crane boom is generally made of manganese steel, which is a high-strength steel, resistant to impact, abrasion, and extrusion, and is suitable for use under harsh working conditions. The experimental design of this article is to detect the quality of manganese steel materials, such as surface holes, oil stains, scratches, protrusions, depressions, and deformations. This article uses image detection technology to detect the quality of manganese steel materials for crane booms and reconstruct manganese the three-dimensional shape of the steel material can complete the inspection of the quality of the manganese steel material. The crane manganese steel material detection frame designed in this paper is shown in Figure 3:

Two projectors are controlled by a computer to project sinusoidal images on the upper and lower surfaces of the manganese steel material, and the two area CCD cameras are used to shoot the moiré images on the upper and lower surfaces of the manganese steel material vertically, and then the computer receives the clouds captured by the CCD camera. We pattern the image and then simultaneously realize the reconstruction, storage, and display the three-dimensional information of the manganese steel material. CMOS has multiple charge-voltage converters and row switch control, readout is much faster, and most high-speed cameras above 500fps are CMOS cameras. The main parameters of the equipment are shown in Table 2.

The distance between the area CCD camera and the projector is 250 mm, and the distance between the projector and the reference plane is 500 mm. The length of the actual material represented by the photographed image is 330 mm, so that the resolution of the photographed image can be guaranteed to be 0.1 mm/pixel ∗ 0.1 mm/pixel.

3.2. Data Collection. The image information received by the computer is extracted and processed, and the processed

Table 1: Common crane boom materials.

Metallic material	Safety factor	Allowable compressive bending stress	Allowable shear stress	Allowable end face to withstand stress
Q235	1.48	153.2	82.4	242.3
Q345	1.48	174.4	102.5	265.1
20	1.48	116.5	76.8	199.7
45	1.48	188.3	134.6	294.8
40Cr	1.48	268.7	159.9	368.5
20Cr	1.48	330.2	178.7	386.4

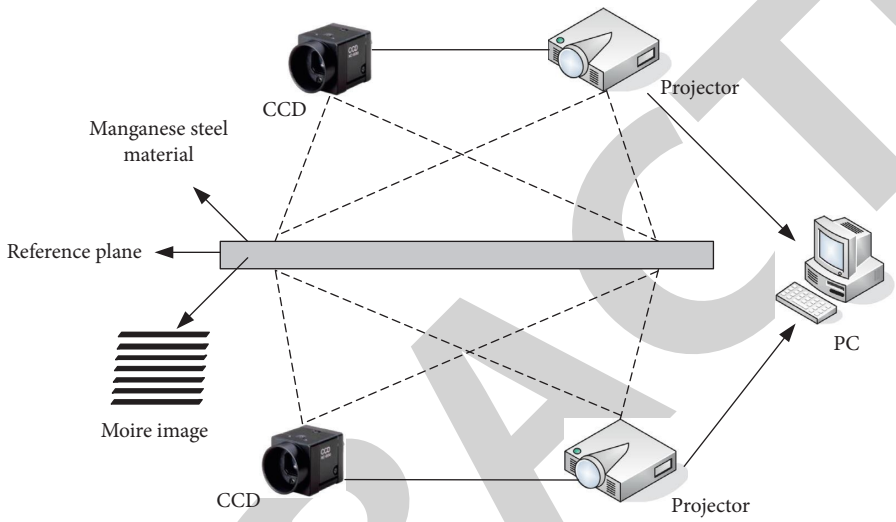

Figure 3: Quality inspection of manganese steel material for crane boom.

Table 2: Device parameters.

Equipment	Configuration	Resolution	Parameter
PC	Intel i7 quad-core processor	12G memory	64 bit Windows 7 operating system
CCD	Horizontal resolution: 3300 pixel	The vertical resolution is: 2500 pixel	The highest frame rate: 10.3fps
Projector	Standard resolution: 1280 ∗ 800	The highest resolution: 1600 ∗ 1200	Brightness: 3700 lumens

image is studied and analyzed, and the spatial frequency, arithmetic mean and gray standard deviation of the image are used as training parameters. After the preprocessing of the image, the next step is to analyze the image. Only after the image analysis can the information in the image be accurate. In the actual operation, some structures and features of the image are extracted and measured, and then, the required information is obtained to obtain the complete image information parameters.

4. Inspection and Analysis of Crane Boom Material Quality Based on Image-Based Precision Measurement

4.1. Three-Dimensional Reconstruction Analysis of the Arm Tube Material. In order to accurately reconstruct the three-dimensional contour of the crane boom material, obtaining high-quality moiré images is the key to the three-dimensional reconstruction of the boom material. After eliminating the distortion of the CCD camera lens, the moiré image on the surface of the arm barrel material is taken. The obvious sinuosity of the captured moiré image is an important feature of high-quality moiré images. The gray value comparison result of the collected moiré image is shown in Figure 4.

The standard sinusoidal moiré projected by the digital projector is deformed for the first time after being projected by the projector. At this time, the moiré image will be further distorted. It is taken by the CCD camera (the distortion produced by the lens when the CCD camera is taken has been eliminated by calibration); the moiré image is further deformed, and the gray value of the moiré image finally collected is better.

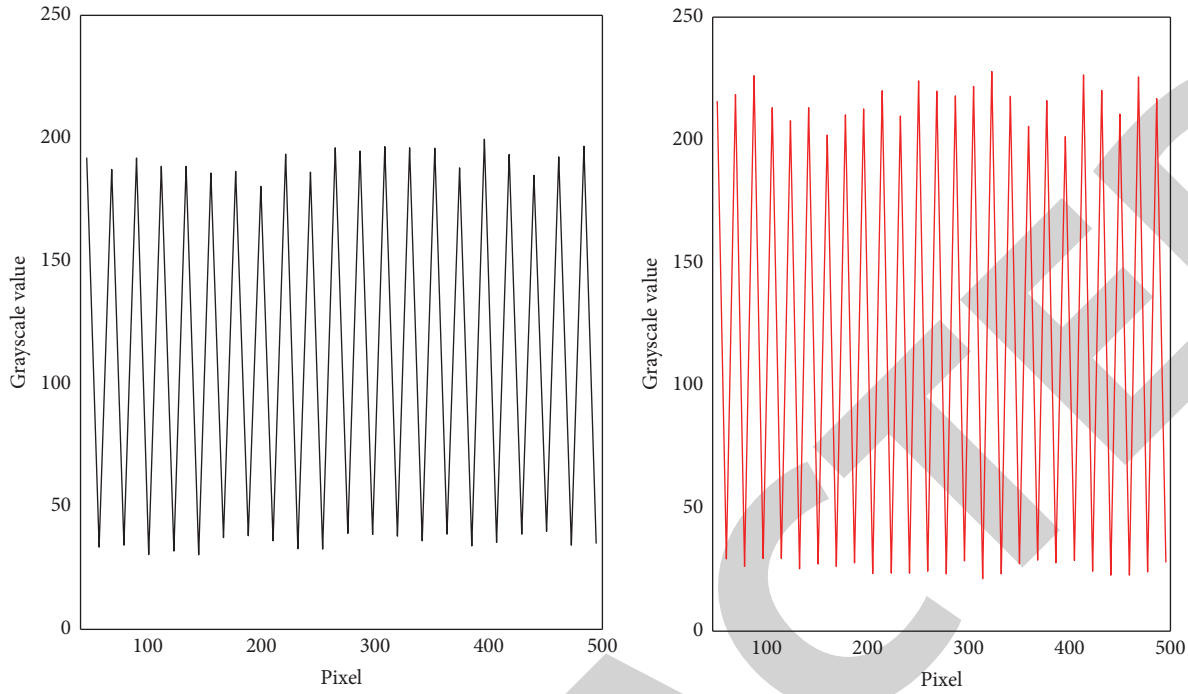

Figure 4: Image gray value comparison.

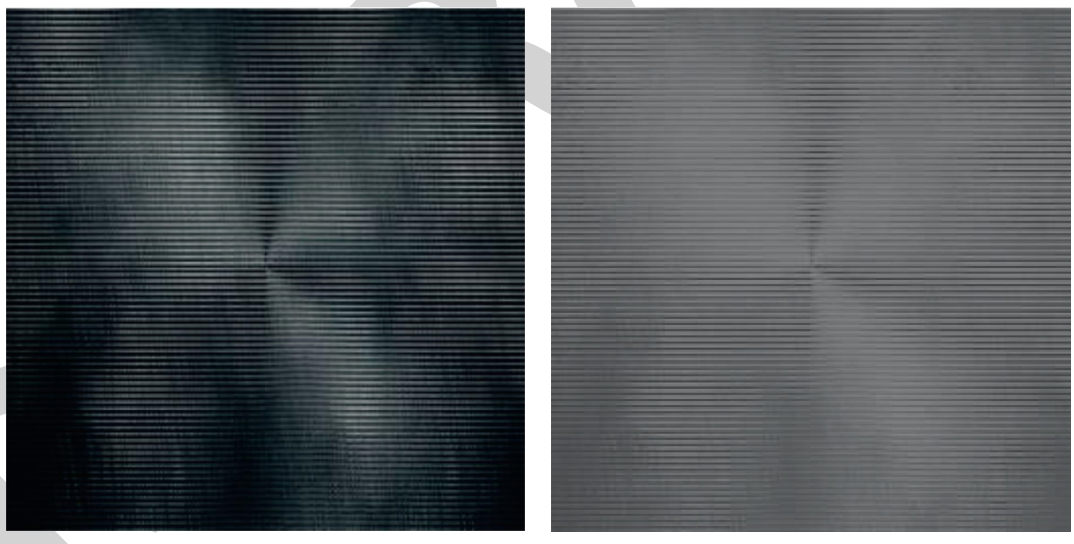

(a) (b)

Figure 5: Comparison chart of arm tube materials after grayscale transformation. (a) The original image. (b) Grayscale processed image.

Each method can expand some features of the grayscale image, and some features can be reduced, so it is extremely important to choose a suitable method to deal with the surface roughness. In the actual image, there are always some unsatisfactory black or white images, you can use the grayscale transformation stretching to adjust and correct the image, as shown in Figure 5.

In the image processing method, the grayscale transformation is selected to process the image. The essence is the logarithmic transformation. In the internal calculation process, it is actually the higher compression processing in the image and the lower grayscale stretching processing. Through the grayscale stretching transformation, the low grayscale of the image can be emphasized.

Figure 6 shows the image grayscale transformation histogram of the crane boom material. In combination with Figure 5, it can be seen that the image can be well corrected and adjusted by grayscale stretching.

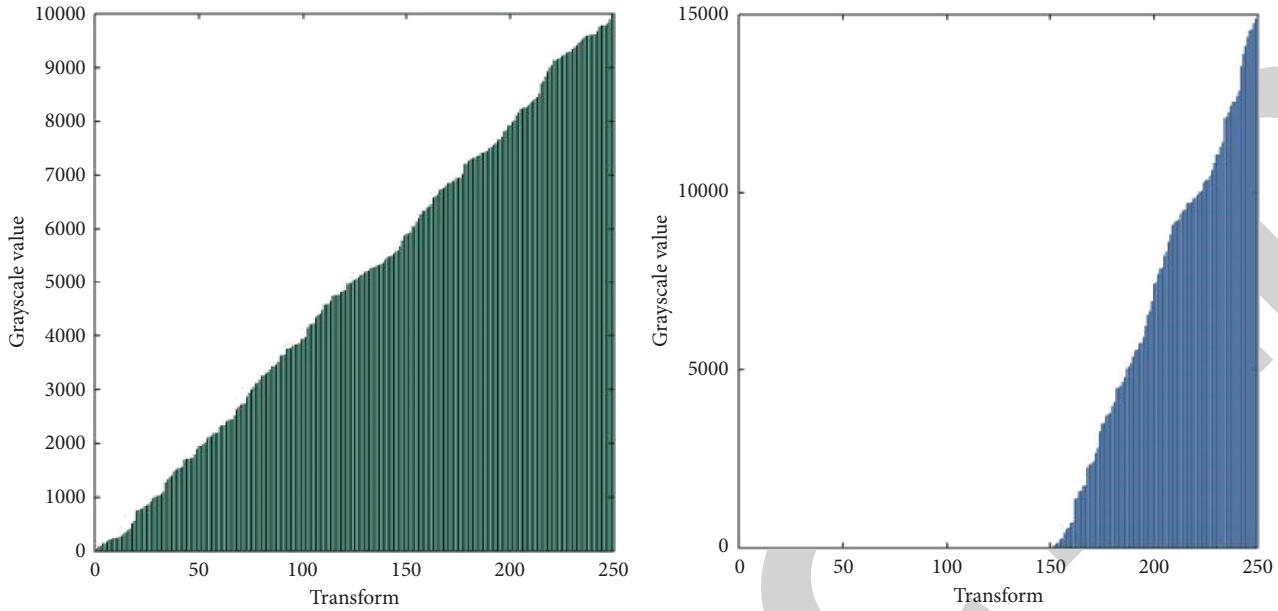

Figure 6: Contrast histogram of original image after grayscale transformation.

Table 3: Surface defect measurement results.

	Wavelet transform	
Moire resolution	Reconstruction error (mm)	Pixel
4	0.01	100
8	0.01	200
16	0.015	300
32	0.015	400

4.2. Thickness Measurement Accuracy of the Arm Tube Material. In order to study the influence of moiré resolution on the accuracy of object reconstruction, different moiré periods are simulated to project the material, and wavelet transform profilometry is used to reconstruct images with different moiré resolutions to analyze the moiré resolution. The influence of rate on the accuracy of object reconstruction. Pixel error, resolution is shown in Table 3:

For the thickness reconstruction error, when the moiré resolution is 4 to 15, the simulation results show that the error is 0.01 mm; when the moiré resolution reaches 16, the simulation error increases to 0.015 mm. It can be seen that blindly increasing the moiré resolution cannot reduce the thickness error. The surface error of the material must be that the higher the resolution of the moiré, the smaller the surface error. Therefore, this paper chooses the image with a moiré resolution of 10 for three-dimensional reconstruction, so that the thickness error is the smallest and the surface error can also be controlled within an appropriate range.

Figure7 can be obtained by Fourier transform of the cross-section of the boom barrel material in Figure 8. Frequency is low, it can be seen as defects after Fourier transform can only affect the Fourier transform of the zero frequency; therefore, the thickness of the arm cylinder material information and defect information is included in the zero frequency; the pulse error is included in the fundamental frequency, so as long as through a low-pass filter to filter out the fundamental frequency keep zero frequency, can eliminate the error. Meanwhile, the material thickness information and defect information of the boom barrel are retained.

4.3. Calculation and Analysis of the Surface Roughness of the Arm Tube Material. The material surface image is grayscaled, and then, through preprocessing, the grayscale distribution of the picture is obtained. According to the grayscale distribution, three sampling lines are drawn randomly on the picture to extract the texture features as shown in Figure 9.

In the gray image, the gray value of the image can reflect the surface condition of the parts according to the optical properties, so the surface roughness value of the workpiece surface can be calculated according to the gray value. Moreover, the gray value in the image can also be used to indicate the degree of undulation of the surface contour of the part, which can be used as the texture feature of the image. In the actual calculation and analysis, according to the traditional surface roughness evaluation parameters, the surface contour line of the simulated surface roughness is calculated as shown in Figure 10.

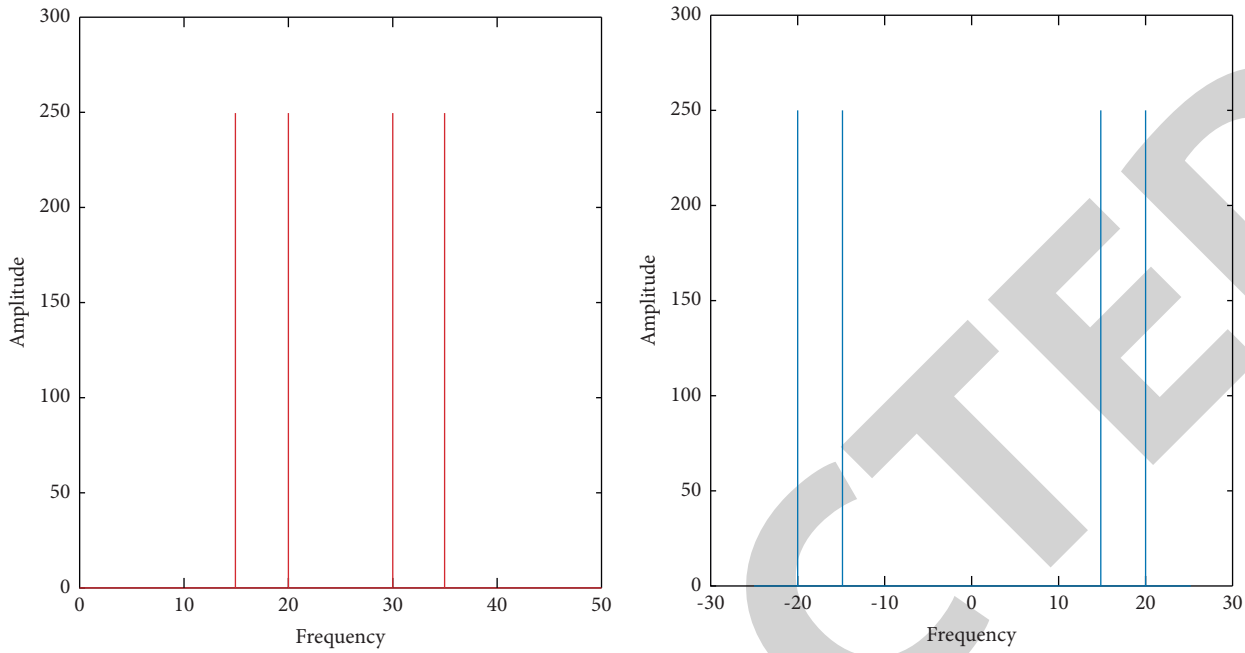

Figure 7: Spectrum comparison chart.

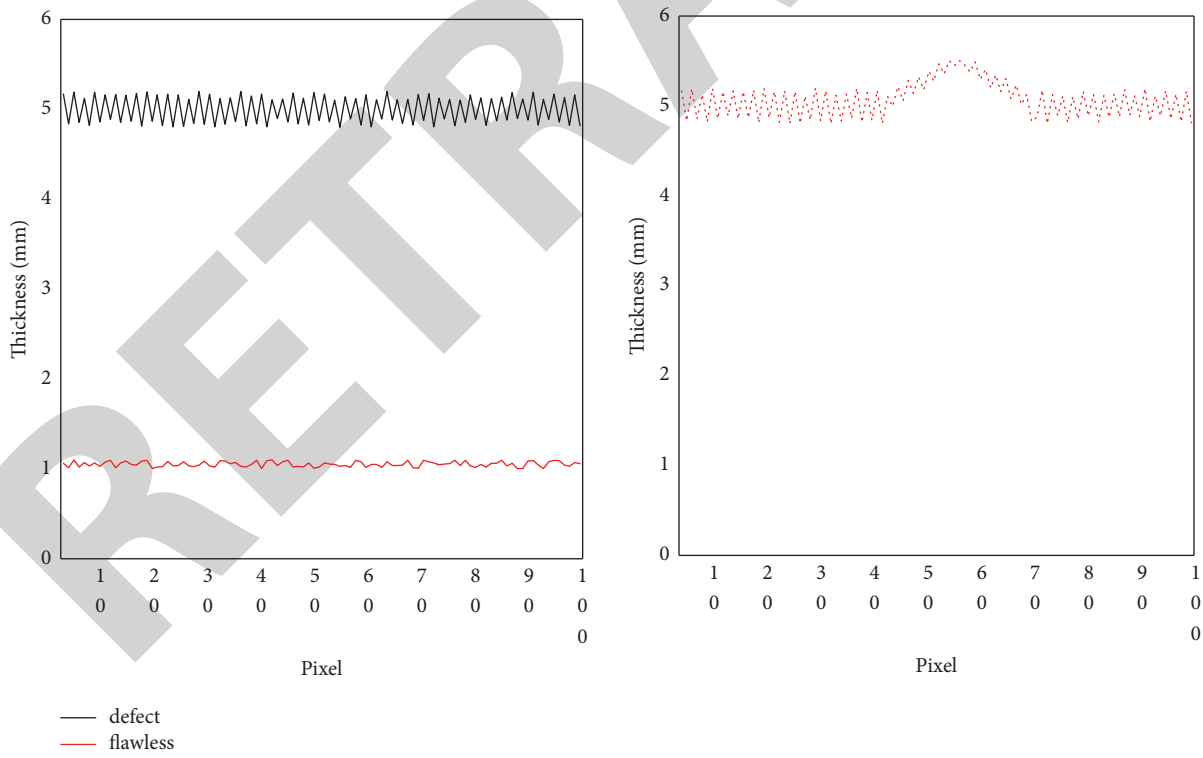

Figure 8: Comparison chart of cross-section error of arm tube material.

According to Figure 10, two data lines are taken from the preprocessed picture, and then combined by the gray value to obtain two contour lines, which can be observed through the two contour lines. The processing traces are the same, and the phase is almost at the same position.

By calculating and analyzing the image data, substituting the data to minimize the variance, the surface roughness of

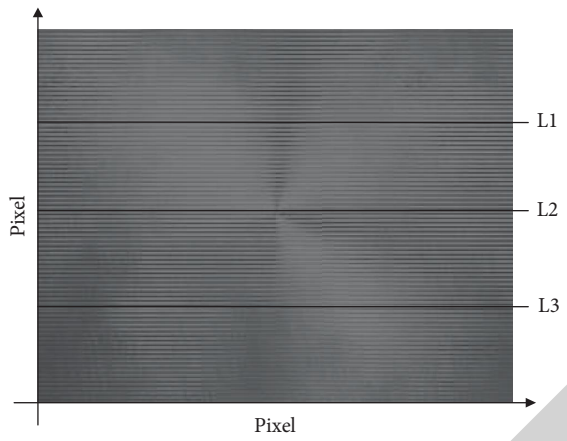

Figure 9: Partial enlarged view of the material surface.

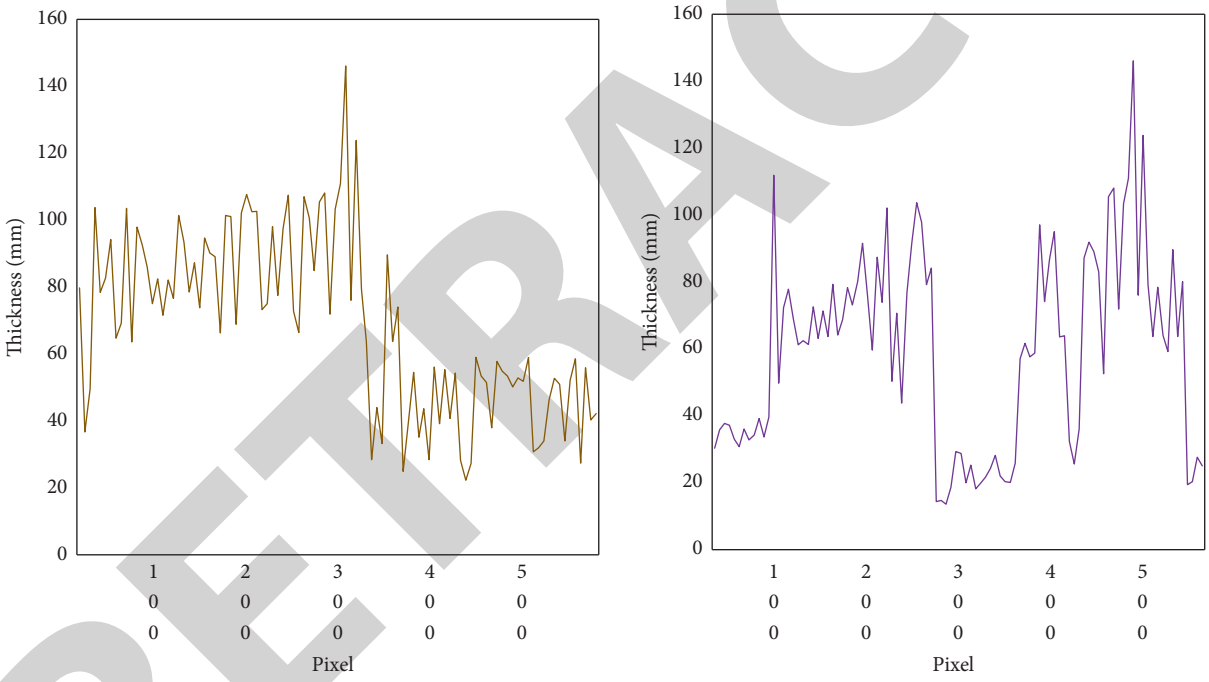

Figure 10: Material surface contour.

Table 4: Parameter evaluation result.

Parameter evaluation	R	F	df1	df2	Significance	Constant	B1
Linear	0.951	565.143	1	10	0	−0.131	0.021
Logarithm	0.914	109.477	1	10	0	−1.162	0.312
Index model	0.896	99.12	1	10	0	0.029	0.061

the arm tube material can be calculated. Judging from the evaluation results of the parameters in Table 4, the significance of the linear, logarithmic, and exponential modes is 0, which has obvious significance. Therefore, the grayscale image can be very suitable for calculating the surface

Table 5: Thickness measurement results of two methods.

Material sample	Wavelet transform measurement results	Measurement results of the method in this paper
Area 1	5.98	5.96
Area 2	6.00	6.01
Area 3	5.97	6.00
Area 4	5.98	6.02
Area 5	6.03	6.02
Area 6	6.02	5.94
Area 7	5.96	6.00
Area 8	6.01	6.01

roughness. For example, a very common compression method in AIX is to convert to a.tar compressed format file.

4.4. Judgment on the Universality of the Appearance Quality Monitoring of Crane Boom Materials. In order to verify the universality of the method proposed in this paper, a piece of material is evenly divided into 8 different areas for thickness measurement as shown in Table 5. All measurement results are compared with the wavelet transforms measurement results.

Table 5 displays a comparison between the average value of the material thickness measurement results based on the wavelet transform profilometry and the average value of the material thickness results measured by the method in this paper. As shown in the table, the wavelet transform measurements were 5.98 for Area 1, 6.00 for Area 2, 5.97 for Area 3, and 5.98 for Area 4. The unit of the measured results in the table is mm. Therefore, it can be concluded that the measurement accuracy of the material thickness of the method in this paper reaches 98.1%, and it can detect surface defects with a minimum size of 0.3 mm.

5. Conclusions

This paper mainly studies the detection technology of crane boom material quality based on image-based precision measurement. The basic image of crane boom material is collected by CCD camera, and the image is preprocessed; then, the image is analyzed to obtain the information in the accurate image. Then, some structures and features of the image are extracted and measured to obtain complete image information parameters. The article analyzes the image preprocessing, introduces the image noise reduction, simplifies the algorithm using Fourier mapping, and conducts experiments. Specific experiments verify the practicability of the method used in this paper, verify the accuracy of the crane boom material quality detection, and verify the universal applicability of the method. The research on the method of measuring the quality of crane boom materials is not only of great significance for improving the appearance quality of materials but also has a certain reference significance for the subsequent noncontact online measurement of the quality of crane boom materials. There are still shortcomings in the research of this paper, such as the image processing problem. After obtaining a high-quality image, it is necessary to calculate the phase value of the image and the phase of the unfolding truncation, but the calculation result will produce periodic errors. We hope to solve this problem in follow-up research. The features in the images can be developed as criteria in future experiments to better obtain target information for the arm tube material.

Data Availability

Data sharing is not applicable to this article as no new data were created or analyzed in this study.

Conflicts of Interest

The authors declare that they have no conflicts of interest.

Acknowledgments

This work was supported by the scientific research project of Hunan Provincial Department of Education, Project number: 20A287.

References

[1] J. Li, L. Bai, W. Gao et al., "Reliability-based design optimization for the lattice boom of crawler crane," *Structures*, vol. 29, no. 2, pp. 1111–1118, 2021.

[2] C. Trevino and M. Abdel-Raheem, "Discussion of "location optimization of tower crane and allocation of material supply points in a construction site considering operating and rental costs" by zahra sadat moussavi nadoushani, ahmed W. A. Hammad, and ali akbarnezhad," *Journal of Construction Engineering and Management*, vol. 144, no. 11, pp. 070180011–070180013, 2018.

[3] F. Yao, W. Meng, J. Zhao, Z. She, G. Shi, and H. Liu, "Buckling theoretical analysis on all-terrain crane telescopic boom with n-stepped sections," *Journal of Mechanical Science and Technology*, vol. 32, no. 8, pp. 3637–3644, 2018.

[4] B. Sun, J. Zhu, L. Yang, S. Yang, and Z. Niu, "Calibration of line-scan cameras for precision measurement," *Applied Optics*, vol. 55, no. 25, pp. 6836–6843, 2016.

[5] H. Zemann, D. Semrad, and H. Paul, "Precision measurement of the/gb-spectrum shape of 32P," *Nuclear Physics A*, vol. 175, no. 2, pp. 385–395, 1971.

[6] P. Yuan and D. Huang, "A high-reliable and high-precision algorithm of angle measurement for UAV airborne photoelectrical detection system," *International Journal of Precision Engineering and Manufacturing*, vol. 20, no. 11, pp. 1885–1891, 2019.

[7] Z. Jing, J. Zhao, and W. Hui, "Precision position measurement of linear motors mover based on temporal image correlation," *IEEE Transactions on Instrumentation and Measurement*, no. 99, pp. 1–10, 2018.

[8] R. Davis, "Science and precision measurement," *Ieee Instrumentation & Measurement Magazine*, vol. 20, no. 1, pp. 8–10, 2017.

[9] D. A. Masterenko and V. I. Teleshevskii, "Features of numerical processing of measurement information for high-precision linear and angular measurements," *Measurement Techniques*, vol. 59, no. 12, pp. 1254–1259, 2017.

[10] Z. Wang, Z. Zhang, and Y. Zhao, "High-precision measurement of tiny difference frequency via weak value amplification," *The European Physical Journal D*, vol. 75, no. 9, pp. 238–247, 2021.

[11] Z. Dong, X. Sun, and W. Liu, "Precision measurement method of free-form curved surfaces based on laser displacement sensor," *Yi Qi Yi Biao Xue Bao/Chinese Journal of Scientific Instrument*, vol. 39, no. 12, pp. 30–38, 2018.

[12] H. G. Min, D. J. Kang, K. J. Kim, and J. H. Park, "New non-contact measurement method of deformation at tensile test of thin film via digital image correlation technique," *International Journal of Precision Engineering and Manufacturing*, vol. 18, no. 11, pp. 1509–1517, 2017.

[13] T. H. Yan, Y. Su, and Q. C. Zhang, "Precise 3D shape measurement of three-dimensional digital image correlation for complex surfaces," *Science China Technological Sciences*, vol. 61, no. 1, pp. 68–73, 2018.

[14] J. Zhao, Y. Zhou, J. Zhao, X. Jiang, and K. Gong, "Rapid-precision position measurement of linear motor mover based on joint spatial phase method," *IEEE Transactions on Industrial Informatics*, vol. 16, no. 7, pp. 4333–4343, 2020.

[15] Y. Ma, X. Liu, and D. Xu, "Precision pose measurement of an object with flange based on shadow distribution," *IEEE Transactions on Instrumentation and Measurement*, vol. 69, no. 5, pp. 2003–2015, 2020.

[16] J. Li, F. Zhao, X. Wang, F. Cao, and X. Han, "The underground explosion point measurement method based on high-precision location of energy focus," *IEEE Access*, vol. 8, no. 99, pp. 165989–166002, 2020.

[17] J. H. Kim, Y. G. Jung, and S. C. Huh, "The stability analysis of offshore lattice boom crane," *Journal of the Korean Society for Power System Engineering*, vol. 22, no. 1, pp. 25–33, 2018.

[18] G. Li and M. Wang, "Morphological analysis of the combination structure of boom-forestay of the crane based on transfer matrix method," *International Core Journal of Engineering*, vol. 5, no. 10, pp. 258–264, 2019.

[19] S. Zhang, B. Li, F. Ren, and R. Dong, "High-precision measurement of binocular telecentric vision system with novel calibration and matching methods," *IEEE Access*, vol. 7, no. 99, pp. 54682–54692, 2019.

[20] W.-J. Tao, X. Liu, X. C. Hong, and L. Z. Hao, "Study on precision measurement of hi-purity monocrystal silicon material density difference at sub-ppm level," *Journal of Nanoelectronics and Optoelectronics*, vol. 12, no. 11, pp. 1295–1300, 2017.

[21] Q. Zhou, Q. Wu, and X. Xiong, "Periodic topology optimization design of tower crane boom," *Tongji Daxue Xuebao/Journal of Tongji University*, vol. 45, no. 10, pp. 1498–1505, 2017.

[22] J. Griffin, *Material-Handling Boom. Underground construction*, vol. 73, no. 11, p. 17, 2018.

[23] F. Babar Khan, "Automatic quality inspection of bakery products based on shape and color information," *Journal of Harbin Institute of Technology*, vol. 05, no. 175, pp. 92–100, 2017.

[24] W. Wang, E. Lin, D. Zhang, and B. Crane, "Onyx embolization material extrusion in the middle ear," *Otology & Neurotology*, vol. 40, no. 8, pp. e847–e849, 2019.

[25] T. Klinger and M. Lanzendorf, "Moving between mobility cultures: what affects the travel behavior of new residents?" *Transportation*, vol. 43, no. 2, pp. 243–271, 2016.

[26] F. Franceschini, M. Galetto, G. Genta, and D. A. Maisano, "Selection of quality-inspection procedures for short-run productions," *The International Journal of Advanced Manufacturing Technology*, vol. 99, no. 9-12, pp. 2537–2547, 2018.

[27] P. A. Belan, R. A. G. de Macedo, W. A. L. Alves, J. C. C. Santana, and S. A. Araujo, "Machine vision system for quality inspection of beans," *The International Journal of Advanced Manufacturing Technology*, vol. 111, no. 11-12, pp. 3421–3435, 2020.

[28] A Flora, "Comprehensive quality solutions for nonwovens Uster Technologies now covers fabric inspection as well as contamination control," *China Textiles*, no. 07, pp. 54-55, 2018.

[29] D. Song, Y. G. Oh, and N. Kim, "Study on correlation-based feature selection in an automatic quality inspection system using support vector machine (SVM)," *Journal of Korean Institute of Industrial Engineers*, vol. 42, no. 6, pp. 370–376, 2016.

[30] J. Xu, L. Ding, H. Luo, E. J. Chen, and L. Wei, "Near real-time circular tunnel shield segment assembly quality inspection using point cloud data: a case study," *Tunnelling and Underground Space Technology*, vol. 91, no. SEP, pp. 102998–10299814, 2019.